Applied Surface Science 276 (2013) 521–528

Applied Surface Science

journal homepage: www.elsevier.com/locate/apsusc

Enhanced photocatalytic performance of Hemin (chloro(protoporhyinato)iron(III)) anchored TiO_2 photocatalyst for methyl orange degradation: A surface modification method

L. Gomathi Devi*, M.L. ArunaKumari

Department of Post Graduate Studies in Chemistry, Central College City Campus, Dr. Ambedkar Street, Bangalore University, Bangalore 560001, India

ARTICLE INFO

Article history:
Received 27 November 2012
Received in revised form 16 March 2013
Accepted 19 March 2013
Available online 27 March 2013

Keywords:
Hemin
Methyl orange
Hemin anchored TiO_2
Surface derivatization

ABSTRACT

TiO_2 was prepared by sol–gel method through the hydrolysis of $TiCl_4$ and its surface derivatization was carried out with molecular catalyst like Hemin (chloro(protoporhyinato)iron(III)). Catalyst was characterized by various analytical techniques like UV–vis spectroscopy, FT-IR, FE-SEM and XRD.

The anchoring of Hemin on titania surface is confirmed by FT-IR spectra through the linkage of O═C—O—Ti bond and also by TGA–DSC and elemental analysis. The photocatalytic activity of the surface modified catalyst is tested for the degradation of methyl orange (MO) as a model compound under UV light. The Hemin impregnated TiO_2 (H-TiO_2) in presence of H_2O_2 shows an excellent photocatalytic activity compared to pristine TiO_2, Hemin, H_2O_2, TiO_2/H_2O_2, and Hemin/H_2O_2 systems. The enhancement in the photocatalytic activity is attributed to the presence of iron (III) porphyrin ring on the TiO_2 surface, which reduces the electron–hole recombination rate and also by acting as a mediator for continuous production of enriched concentration of hydroxyl radicals along with various other reactive free radicals.

1. Introduction

Molecular modification of TiO_2 surfaces is a field of high interest in heterogeneous catalysis. A vast literature has emphasized the importance of design and control of interfaces for the development of functional catalytic surfaces [1], but most of the reported studies are concerned with semiconductor modification especially by metal and non-metal particles. Less attention has been paid to the molecular functionalized semiconductor surfaces for the photocatalysis.

In the case of TiO_2 the photocatalytic activity is influenced by a wide variety of factors such as specific surface area, the adsorption affinity and electron–hole recombination process in the bulk and on the surface of the catalyst, intensity and spectral distribution of the illuminating light, crystal morphology, intrinsic solid state defects, pH of the medium, the presence of electron acceptor and the concentration of the pollutants. In addition, operational conditions and constituents in water matrix also influences the overall efficiency of photocatalysis [2]. But the current bottle neck with photocatalysis lies in its low quantum yield, which depends on the ratio of surface charge carrier transform rate to the electron–hole (e^-–h^+) recombination rate. To increase the quantum yield, the recombination rate should be reduced [3], which is achieved in the present work by anchoring the Hemin molecules on to the TiO_2 surface. Hemin is a protoporphyrin IX Fe (III) complex, which is an active part of Hemoglobin. Heme is a prosthetic group present in a large number of biomolecules in living systems performing key biological functions such as oxygen transport, electron transport and many redox processes [4]. This surface modified H-TiO_2 photocatalyst is characterized by UV–vis spectroscopy, XRD, FT-IR, FE-SEM, TGA–DSC and elemental analysis techniques.

2. Experimental

2.1. Materials

Titanium (IV) chloride ($TiCl_4 \geq 99.9\%$), Hemin, methyl orange and acetonitrile (HPLC grade) were obtained from Merck Chemicals Limited, hydrogen peroxide (30%, w/v) from Sisco-Chemical industries and dimethyl sulfoxide from SD Fine Chemicals. Double distilled water was used throughout the experiment.

2.2. Catalyst preparation

Anatase TiO_2 was prepared by sol–gel method through the hydrolysis of $TiCl_4$ as mentioned in earlier literature [5].

* Corresponding author. Tel.: +91 80 22961336.
E-mail address: gomatidevi_naik@yahoo.co.in (L.G. Devi).

0169-4332/$ – see front matter © 2013 Elsevier B.V. All rights reserved.
http://dx.doi.org/10.1016/j.apsusc.2013.03.127

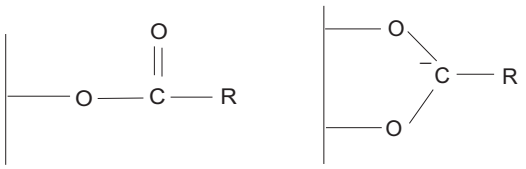

Scheme 1A Scheme 1B

Scheme 1. (A) Uncomplexed carboxylic acid linkage and (B) complexed carboxylate linkage.

Accurately weighed TiO_2 was immersed in the 5 μM Hemin solution made up of 1:1 mixture of dimethyl sulfoxide and acetonitrile (DMSO/CH_3CN), at pH 4 for a day and then centrifuged to remove the solvent. The resulting Hemin anchored TiO_2 (H-TiO_2) powder was dried at room temperature until solvent volatilizes completely. The anchoring of Hemin molecule on the surface of semiconductor occurs through the —COOH functional group. As reported in the literature, the mode of binding depends on the interfacial pH [6], since ionization states of TiO_2 surface can either be protonated or deprotonated under acidic and alkaline pH values. In acidic pH condition the Hemin molecule is bound to TiO_2 surface through uncomplexed carboxylic acid linkage, where as in alkaline conditions it is bound through complexed carboxylate linkage as shown in Scheme 1A and B. Hemin binding to TiO_2 surface involves interlinkage of TiO_2 nanoparticles through —COOH linkage which may lead to agglomeration. At basic pH conditions more interlinking of TiO_2 particles is expected due to complexed carboxylate linkage. The OH group bound to TiO_2 surface deprotonates the carboxylic acid group of Hemin leading to the formation of a water molecule, thereby increasing the adherence of the Hemin molecule onto the TiO_2 surface [7].

2.3. Characterization

The powder X-ray diffraction (PXRD) patterns were obtained for the samples using Philips powder diffractometer PW/1050/70/76. The diffraction patterns were recorded at room temperature using Cu Kα radiation with Ni filter in 2θ range 20–80° at a scan rate of 2° per min. To study the light absorption characteristics of the photocatalyst, the UV-Visble absorption spectra were recorded using Shimadzu-UV 3101 PC UV-VIS-NIR UV-Visible spectrophotometer in the range 200–800 nm. The baseline correction was done using a calibrated sample of $BaSO_4$. FT-IR spectra were obtained using NICOLLET IMPACT 400 D FTIR spectrometer. Surface morphology was analyzed by FE-SEM analysis using ULTRA 55 Field Emission Scanning Electron microscope (Karl Zeiss) with EDS. Thermogravimetric analysis was carried out using TA instrument, SDT analyzer model Q 600 in the temperature range of 25–1000 °C under nitrogen atmosphere with a heating rate of 20 °C min^{-1}. Elemental analysis was obtained with an ELEMENTAR Vario Micro Cube CHNS analyzer.

2.4. Photocatalytic degradation procedure

The photocatalytic activity of TiO_2 and H-TiO_2 were evaluated by the photocatalytic decomposition of methyl orange (MO) in an aqueous suspension using a photochemical reactor consisting of artificial UV light source of 125 W medium pressure mercury vapor lamp with the photon flux of 7.70 mW/cm^2 (as determined by ferrioxalate actinometry) whose wavelength peaks around 350–370 nm is used. Pyrex glass reactor of size of 1 l capacity whose surface area is 176 cm^2 is directly exposed to the light source in open air condition. The entire photo reactor system is maintained at 25 °C using thermostat. In a typical experiment, 250 ml of 10 ppm dye solution was used along with 150 mg of catalyst and optimum amount of oxidant. The light was focused on the solution at a distance of 29 cm and the dye concentration in the aqueous phase was estimated using an UV–vis spectrophotometer. The activity of H-TiO_2 was compared with various reaction systems like (i) only with pure TiO_2, (ii) with Hemin, (iii) with H_2O_2, (iv) TiO_2/H_2O_2 and (v) Hemin/H_2O_2. A blank experiment containing only the substrate MO in the absence of photocatalyst with illumination was performed in order to determine the contribution of the photolysis.

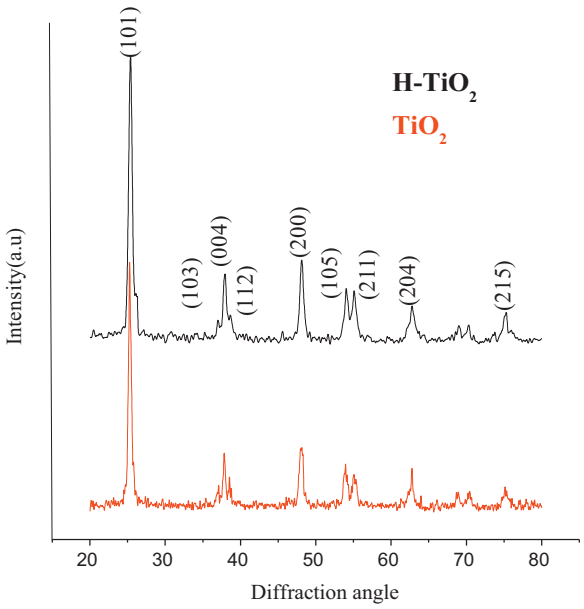

Fig. 1. XRD pattern of TiO_2 and H-TiO_2.

3. Results and discussion

3.1. PXRD studies

Fig. 1 shows the PXRD patterns of TiO_2 and H-TiO_2. Both the samples show peaks at 2θ values of 25.3° (1 0 1), 38° (1 1 2), 48° (2 0 0), 54° (1 0 5), 55° (2 1 1), 62° (2 0 4) and 68° (1 1 6) corresponding to anatase phase. The numbers in the parenthesis represents *hkl* values. From PXRD patterns it can be concluded that the structure of Hemin anchored TiO_2 remains unchanged compare to the bare TiO_2, indicating that the anchoring process did not destroy the characteristic crystal structure of TiO_2.

3.2. UV-Visble absorption spectroscopy

Fig. 2 shows the absorption spectra spectra of bare TiO_2 and H-TiO_2. The absorption spectrum of the TiO_2 includes a single broad intense absorption around 400 nm because of the charge-transfer from the VB (chiefly formed by 2p orbital's of the oxygen atoms) to the CB (mainly is formed by 3d t_{2g} orbital's of the Ti^{4+} cations) [8–10]. In the case of H-TiO_2, absorption spectral findings revealed a red shift in the absorption onset value to 480 nm and high intensity absorption at 280 nm. The appearance of red shift is due to anchoring of Hemin on TiO_2 surface and the observed high intensity absorption at 280 nm may be due to the presence of double bonds in porphyrin ring of Hemin molecule. Inset is an expansion of the Q-band region (500–600 nm) which is the characteristic feature of Hemin [11]. Absorption spectral findings confirm the anchoring of Hemin molecules on the surface of TiO_2.

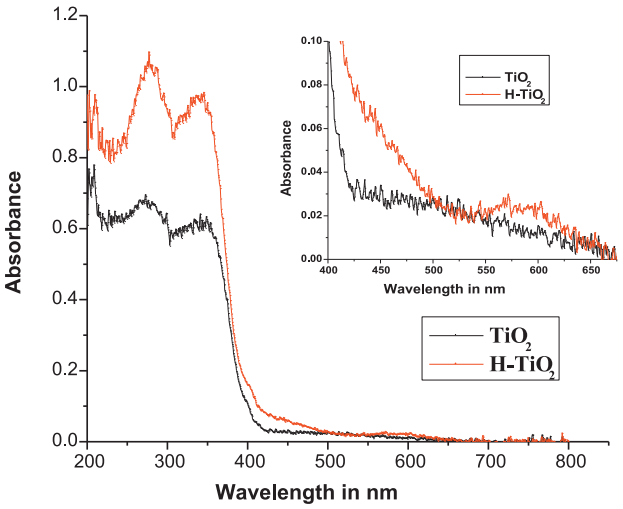

Fig. 2. UV–vis spectra of TiO_2 and H-TiO_2.

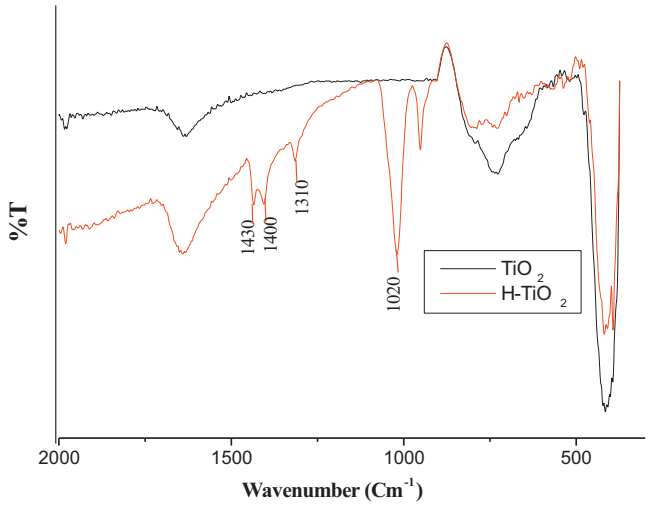

Fig. 3. FTIR spectra of TiO_2 and H-TiO_2.

3.3. FT-IR spectra

The vibrational spectra of the system can be better understood considering the structure of Hemin. It consists of a protoporphyrin (IX) ring system and Fe (III) occupies the centre of its cavity, with a co-ordinated chloride ion as shown in Scheme 2. The Fe (III) center is square pyramidal in geometry, due to the high spin penta co-ordination of ligands. The porphyrin ring has several side chains like carboxyethyl, vinyl, and methyl groups [4].

Anchoring of Hemin was further confirmed by FTIR technique. Fig. 3 shows FT-IR spectra of TiO_2 and H-TiO_2. The spectrum displays two characteristics broad band's centered at 3480 (not shown in figure) and 1640 cm^{-1} which can be assigned to the stretching and bending modes of vibration of adsorbed water or owing to the existence of Ti—OH vibration. A remarkable broad band centered at 735 cm^{-1} is detected which is associated with the stretching mode of vibrations of bridged Ti—O bonds. The spectrum of H-TiO_2 shows an highly intense band at 1020 cm^{-1} due to the C—O stretching vibration and a split peak around 1430–1400 cm^{-1} corresponding to C=O vibrations of surface bound carboxylic acid (to TiO_2) and hydrogen bonded carboxylic acid respectively. Another small peak observed at 1310 cm^{-1} is due to C—O stretching modes. FT-IR study confirms the binding of Hemin molecule to the TiO_2 surface through O=C—O—Ti bond. The broadened peaks observed at 3480 and 1640 cm^{-1} confirms the presence of uncoordinated —COOH group and hydrogen bonded —COOH groups which are still present in the adsorbed Hemin molecules [6].

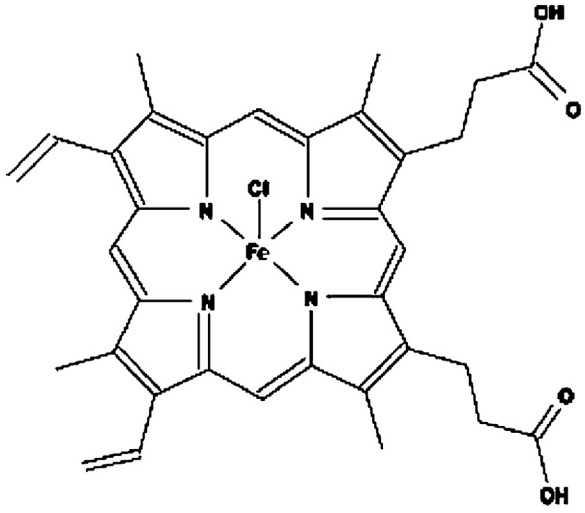

Scheme 2. Structure of Hemin molecule.

3.4. FE-SEM

Fig. 4A and B shows the field emission scanning electron micrographs of TiO_2 and H-TiO_2 respectively. FE-SEM micrograph shows that the powder consists of nano particulates of varying size and shape. The particle size of varies from 19.69 to 29.49 nm and 20.69 to 26.57 nm for TiO_2 and H-TiO_2 respectively. Significant surface modification takes place in the case of H-TiO_2. TiO_2 showed flat structure with smooth surface, whereas H-TiO_2 has rough surface. Particles are agglomerated due to the interlinkage of TiO_2 nanoparticles by —COOH functional groups of Hemin. This indicates the strong adsorption of Hemin molecules on TiO_2 surface. The particle size is determined at three distinct spots and the average value was found to be 21.19 and 23.023 nm for TiO_2 and H-TiO_2 respectively. The increase in particle size of H-TiO_2 is due to the anchoring of bulky Hemin molecule on the titania surface.

4. Photocatalytic degradation studies

4.1. Effect of catalyst concentration

Experiments were done with different catalyst concentrations. The reaction rates were found to enhance linearly as the catalyst concentration increases and later shows exponential behavior. The observed linear increase in the degradation rate may be due to: (i) increase in the number of photons absorbed by catalyst; (ii) increase in the extent of dye molecules adsorption on the catalyst surface; (iii) increase in the number of surface active sites; (iv) increase in the surface area; (v) and also due to increase in the concentration of charge carriers which enhances the generation of hydroxyl radicals [12]. The degradation rate remains almost constant beyond certain limits, which may be due to: (i) the agglomeration of the catalyst particles at higher dosage which covers the part of photosensitive area which hinders the photon absorption and also the dye adsorption process; (ii) turbidity at higher catalyst dosage results in the shadowing effect by decreasing the light penetration depth; and (iii) high degree of scattering by the catalyst particles and increase in the opacity [13,14]. Hence above a certain level, the additional catalyst concentration does not show

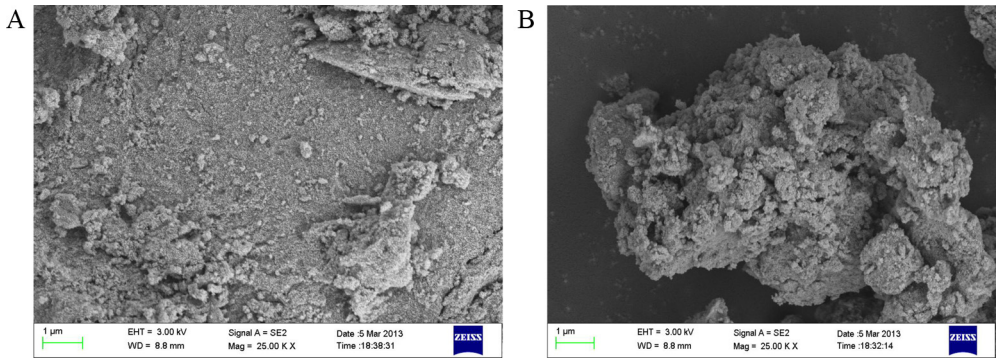

Fig. 4. Field emission scanning electron microscopic images of (A) TiO_2 and (B) H-TiO_2.

any degradation rate enhancement, which is characteristic of all heterogeneous catalysis process [15,16].

4.2. Effect of initial dye concentration

Different concentrations of methyl orange were used ranging from 10 to 100 ppm. Beyond this concentration, degradation rate decreased. It was found that efficiency was maximum for 10 ppm substrate concentration of the dye. It is evident that the photo degradation rate depends on the initial dye concentration, because (i) at higher concentrations, dye might serve as inner filter for shunting the photons away from the catalyst surface; (ii) more number of dye molecules get adsorbed on the catalyst surface thus blocking the surface active sites which are required to absorb the photons; (iii) at high concentrations of dye, the collision probability between dye and oxidizing species decreases which may lead to the decrease in degradation rate [15,17].

4.3. Effect of pH

pH is a complex parameter in a degradation reaction medium as it is related to several factors like: (i) charge on the catalyst surface; (ii) nature of the dye (cationic/anionic/neutral); (iii) magnitude of the substrate adsorption on catalyst surface; (iv) size of the catalyst particle aggregate formed. In general, the adsorption of the pollutant molecule on the catalyst surface is the result of overall balance of different effects including the polar/hydrophilic character of the molecule/substrate, solid surface charge and state. The point of zero charge (pzc) of TiO_2 is widely reported to be 6.25. Thus, the surface charge of TiO_2 will be positive below the pzc and negative above it [18]. Degradation of MO was carried out at 3 different pH values of 3.0, 6.0 and 9.0. The influence of pH for MO dye degradation by H-TiO_2/H_2O_2 shows the following decreasing order; pH: 3.0 > 6.0 > 9.0. This is because at pH 3.0 both Fenton type reaction by active role of iron (III) porphyrin and TiO_2 semiconductor mediated photocatalysis takes place simultaneously. At pH 3.0, dominant photoactive species are produced which results in highest quantum yield of hydroxyl radical along with the regeneration Fe^{2+} ion. This induces efficient dye degradation [19]. On the other hand, at lower pH value the surface of TiO_2 will be positively charged and hence complex formation with negatively charged sulfonate groups of MO through electrostatic force of attraction favors the strong adsorption. With increase in the pH, the rate of adsorption of MO decreases due to the decrease in the positively charged active sites on TiO_2. At alkaline pH values both the catalyst and dye molecules are negatively charged, thus there is a columbic force of repulsion which will not favor the complex formation. This may decrease the degradation rate [20]. At alkaline pH, reactions proceeds partially because of semiconductor mediated photocatalysis.

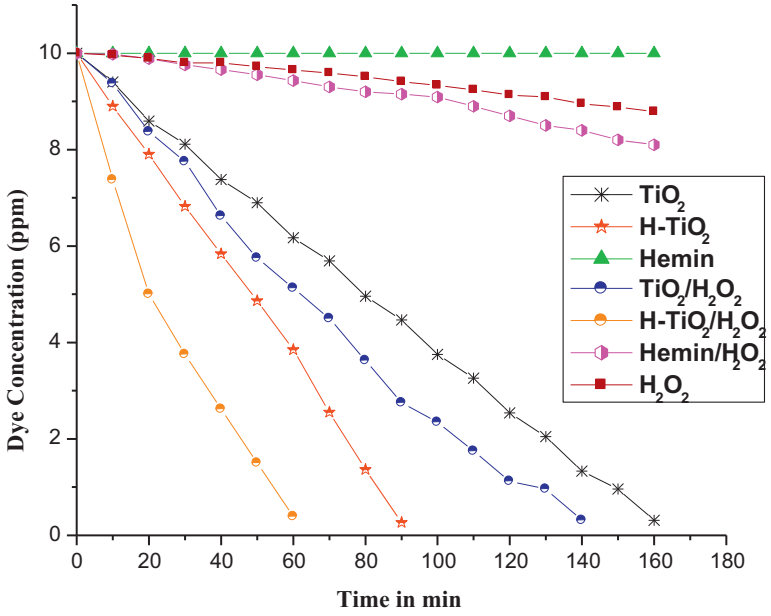

Fig. 5. The plot of concentration of MO versus time under UV illumination for various systems.

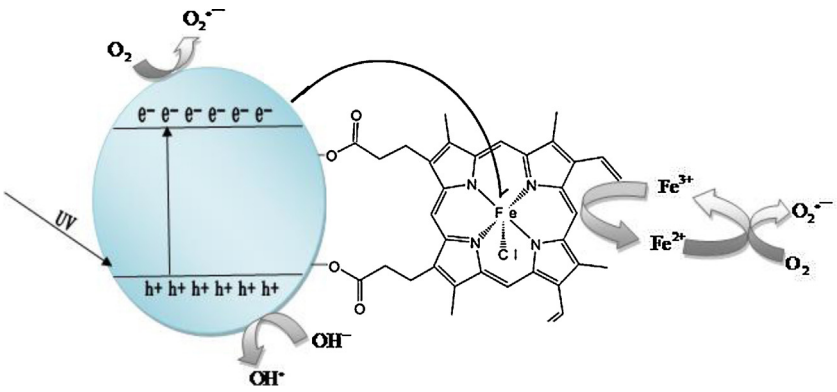

Fig. 6. Mode of photogenerated electron transfer from TiO_2 to Hemin and from Hemin to molecular oxygen.

4.4. Photocatalytic activity

The photocatalytic activity of H-TiO_2 was evaluated in comparison with TiO_2 for the decomposition of MO under UV light irradiation. The extents of MO degradation versus irradiation time intervals for various systems are shown in Fig. 5. The H-TiO_2/H_2O_2 system showed the highest activity for the degradation of MO. This enhancement in photocatalytic activity of H-TiO_2/H_2O_2 system is attributed to the reduced electron–hole recombination rates. On UV illumination charge carriers are generated as shown in Eq. (1).

$$\text{H-TiO}_2 + h\nu \rightarrow \text{H-TiO}_2\,(e^- + H^+) \quad \text{electron–hole generation} \qquad (1)$$

The photogenerated electrons in the conduction band (CB) of H-TiO_2 are transferred in two different pathways (i) the CB electron may be immediately transferred to Fe^{3+} ion present in the Hemin molecule reducing the ferric Hemin to ferrous Hemin as shown in Eq. (2) and Fig. 6, (ii) alternatively the CB electrons can be transferred to molecular oxygen reducing it to super oxide radical anion $O_2^{\bullet-}$ as shown in Eq. (3). The standard redox potential of Fe^{2+}/Fe^{3+} is 0.77 V resides energetically within the forbidden energy gap of TiO_2 [21].

$$\text{H-TiO}_2\,(e^-) + Fe^{3+}\,(\text{Hemin}) \rightarrow Fe^{2+}\,(\text{Hemin})$$
$$\text{electron trapping by Hemin} \qquad (2)$$

$$\text{H-TiO}_2\,(e^-) + O_2 \rightarrow O_2^{\bullet-} \quad \text{electron trapping by oxygen} \qquad (3)$$

$$Fe^{2+}\,(\text{Hemin}) + O_2 \rightarrow O_2^{\bullet-} + Fe^{3+}\,(\text{Hemin})$$
$$\text{electron detrapping by Hemin} \qquad (4)$$

According to crystal field theory, the reduced ferrous Hemin (Fe^{2+}) is relatively unstable due to the loss of d^5 (half filled high spin) electronic configuration and tend to return immediately to Fe^{3+} (d^5) state to attain stable electronic configuration. Subsequently Fe^{2+} could be oxidized to Fe^{3+} by transferring electron to adsorbed O_2 molecule on TiO_2 [22]. Shallow trapping of photogenerated electron by ferric ion of Hemin and detrapping of this electron to attain stable half filled electronic configuration is a continuous cyclic process. Similar mechanism has been proposed in the literature for molecular compounds on TiO_2 interfaces [1,23] as well as Fe (III) doped TiO_2 [3,24–26]. The photogenerated holes can oxidize the dye molecules by the production of hydroxyl radicals, furthermore $O_2^{\bullet-}$ and $OH^\bullet$ produced in Eqs. (3)–(5) being powerful oxidants can also oxidatively degrade the dye.

$$h^+ + OH_{(surf)}{}^- \rightarrow OH_{(surf)}{}^\bullet \qquad (5)$$

$$OH_{(surf)}{}^\bullet + MO \rightarrow CO_2 + H_2O \qquad (6)$$

$$O_2^{\bullet-} + MO \rightarrow CO_2 + H_2O \qquad (7)$$

When H_2O_2 is added to the H-TiO_2 system, there is a remarkable enhancement in the rate of photocatalytic degradation. H_2O_2 alone under UV light was able to degrade the MO to the extent of 7–8%. This is due to the direct photolysis of H_2O_2 under UV light of wavelength around 280 nm, which leads to the formation of reactive hydroxyl radicals. But the yield of such hydroxyl radicals is found to be very low since the wavelength of the light is around 350–370 nm. However when H_2O_2 is added to the H-TiO_2 system, there is a remarkable enhancement in the rate of photocatalytic degradation due to the continuous cyclic process in which Fe^{3+} ion in Hemin is reduced to Fe^{2+} and again Fe^{2+} in turn gets oxidized to regenerate Fe^{3+} along with enriched concentration of hydroxyl radicals and various other reactive free radicals (as shown in Scheme 3) which is responsible for higher efficiency of H-TiO_2. This increase in the activity can be attributed to the active role of Hemin as a co-catalyst and mediator by continuous production of hydroxyl radicals [25–28]. Consequently, the degradation rate is expected to be enhanced, but at very high dosage of H_2O_2, it acts as a powerful hydroxyl radical scavenger (Eqs. (8) and (9)) and hence the rate of degradation decreases [16].

$$H_2O_2 + OH^\bullet \rightarrow HO_2^\bullet + H_2O \qquad (8)$$

$$HO_2^\bullet + OH^\bullet \rightarrow H_2O + O_2 \qquad (9)$$

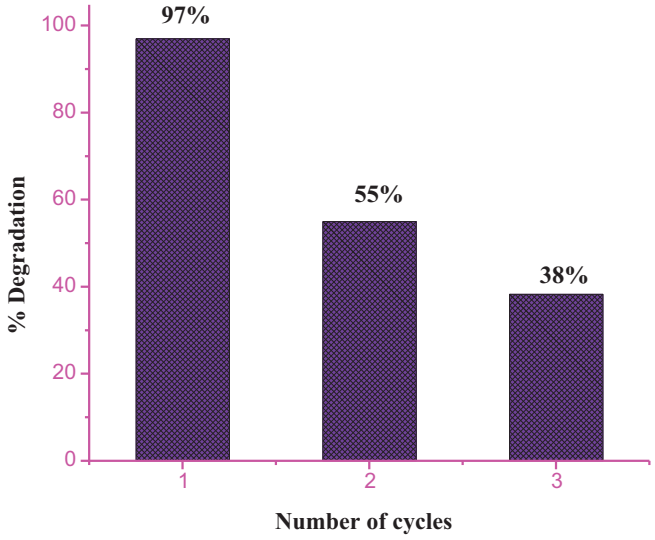

Fig. 7. A plot of percentage degradation versus number of cycles for the reuse of H-TiO_2 under UV illumination for a time period of 60 min.

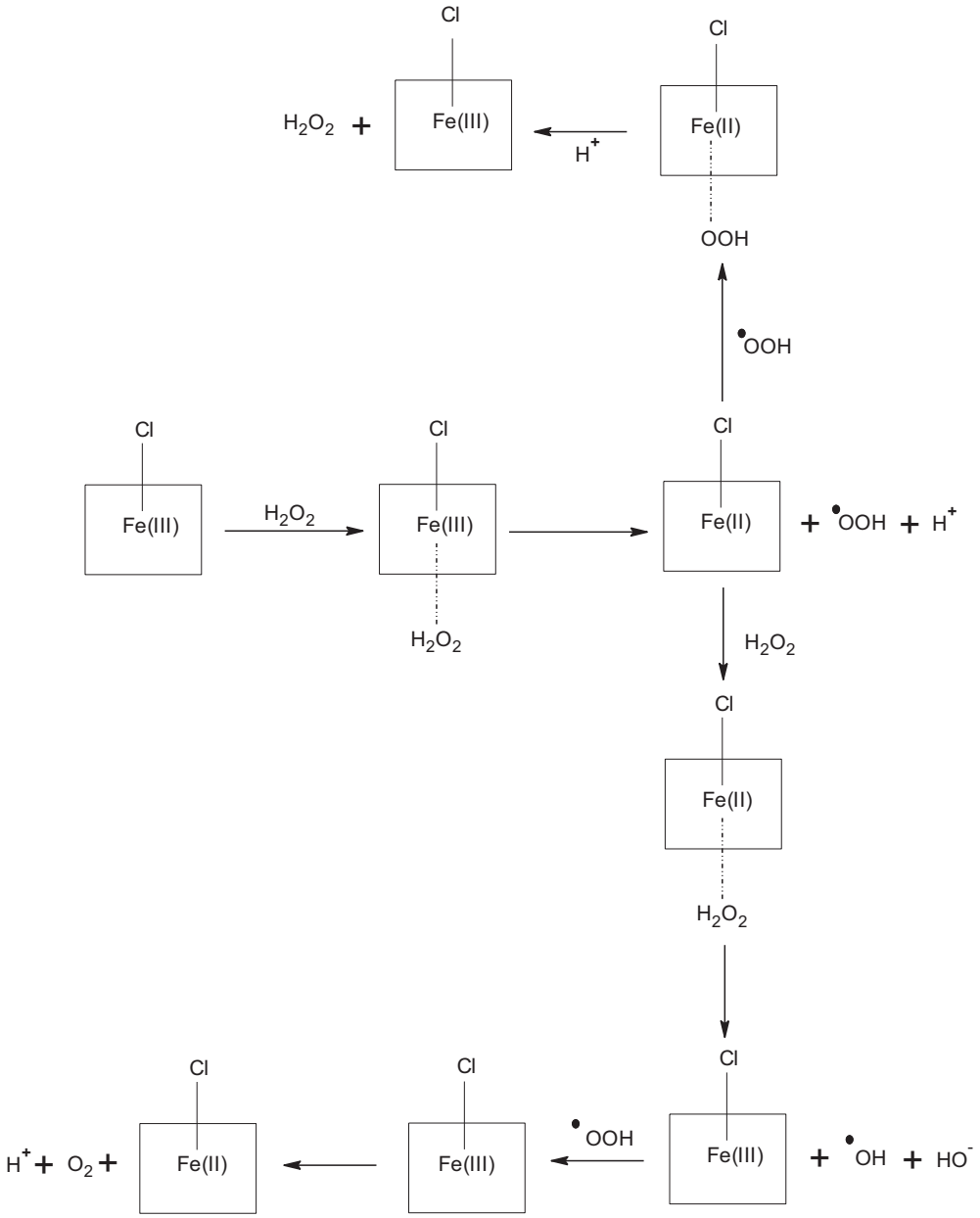

Scheme 3. Schematic representation of the proposed reaction mechanism.

5. Reusability of H-TiO_2 in multiple runs

Experiments were conducted to check the recyclability of H-TiO_2. The catalyst was recycled under same reaction conditions to evaluate the stability of Hemin molecule on TiO_2 surface. After every run, the suspensions were centrifuged and the catalyst was collected, washed thoroughly, and air dried before the next experiment. The regenerated catalyst was used in the photocatalytic degradation experiment and its activity was evaluated. The results obtained are shown in Fig. 7. The reduction in the activity of H-TiO_2 can be accounted to the slight loss of organic content of porphyrin group of Hemin during the course of reaction. These results are further substantiated by the elemental analysis and thermo gravimetric analysis (TGA) of H-TiO_2. The color of the catalyst changes from dark green to pale green when it is reused. The catalyst appears pale cream color in the third cycle and the degradation results are comparable to that of pristine TiO_2. TGA was performed for TiO_2, H-TiO_2, and recycled H-TiO_2 samples. The thermograms (Fig. 8) show a weight loss of 1.7% and 2.6% for TiO_2 and H-TiO_2 respectively. The weight loss in TiO_2 is due to the surface adsorbed water molecules and also due to surface bound hydroxyl groups. The excess weight loss in H-TiO_2, and recycled H-TiO_2 is due to the burning off of organic residues in the porphyrin group of Hemin. The results obtained from elemental analysis are given in Table 1. The total percentage of carbon, hydrogen and nitrogen (CHN) was up to 0.959%. The difference in the weight loss observed in TGA between TiO_2 and H-TiO_2 samples is also 0.9% (1.7–2.6%). The H-TiO_2 catalyst when reused for second time shows a weight loss of

Table 1
Elemental analysis of TiO_2, H-TiO_2 and reused H-TiO_2.

Catalyst	C%	H%	N%	Total %
TiO_2	–	–	–	–
H-TiO_2	0.64	0.299	0.02	0.959
H-TiO_2 (reused)	0.29	0.174	0.01	0.474

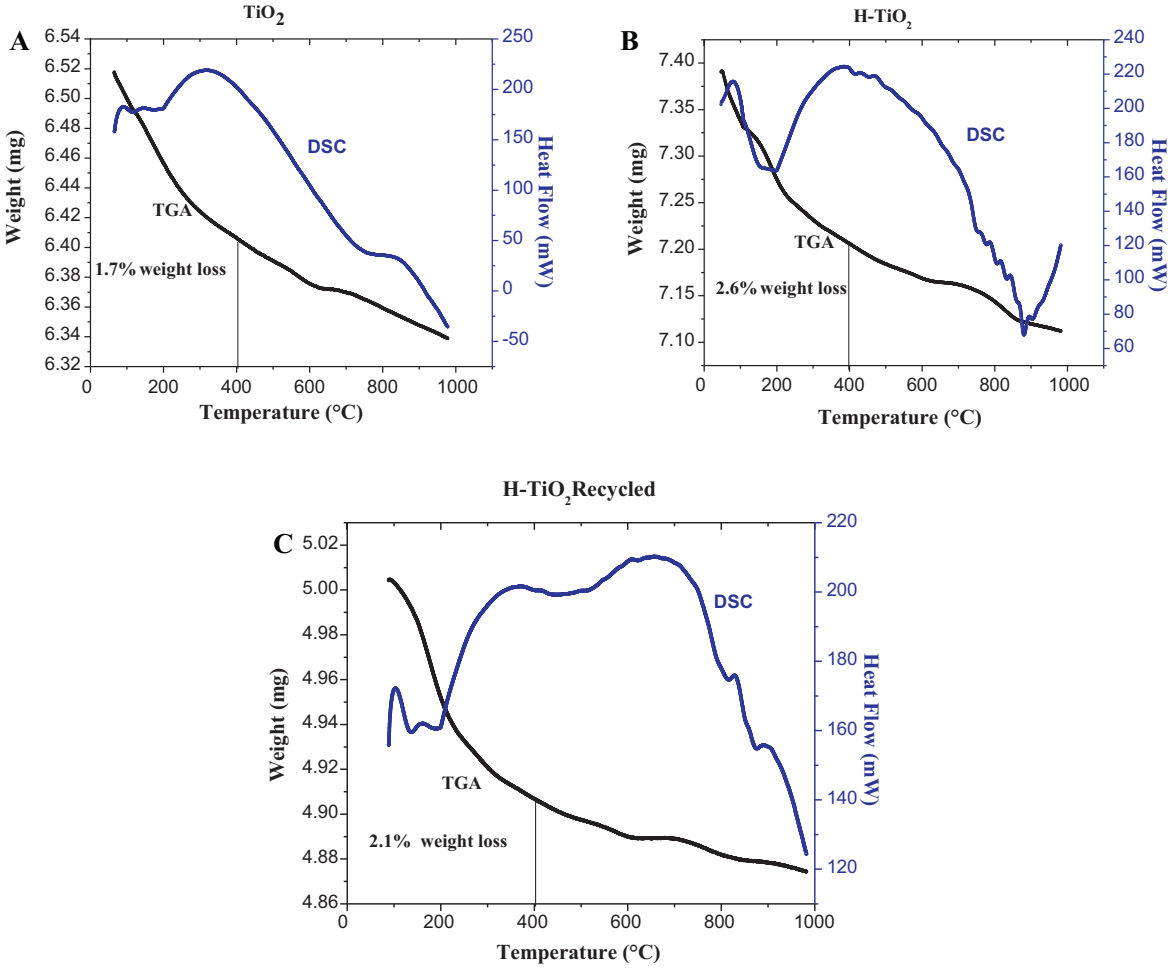

Fig. 8. Thermograms of (A) TiO_2, (B) H-TiO_2 and (C) reused H-TiO_2 from TGA and DSC analysis.

2.1%. This clearly means that there is 0.4% loss of Hemin. The result shows good agreement with elemental analysis.

6. Conclusion

The present work discusses the photochemical behavior of surface modified nanocrystalline TiO_2. Molecular catalyst like Hemin (chloro(protoporhyinato)iron(III)) is anchored to TiO_2 surface by O═C—O—Ti bond. The mode of Hemin molecule binding depends on the interfacial pH. In the acidic media the Hemin molecule is bound to TiO_2 surface through uncomplexed carboxylic acid linkage. The OH group bound to TiO_2 surface deprotonates the carboxylic acid group of Hemin leading to an increase in the adherence of the Hemin molecule onto the TiO_2 surface. The photocatalytic properties of the system were assessed by the degradation of MO. The presence of iron (III) porphyrin on the TiO_2 surface increases the photocatalytic efficiency by three folds with respect to unmodified TiO_2 by reducing the electron–hole recombination rate and also by acting as a mediator for continuous production of hydroxyl radicals in presence of H_2O_2. Shallow trapping of photogenerated electron by ferric ion of Hemin and detrapping of this electron to attain stable half filled electronic configuration is a continuous cyclic process. The reusability of the H-TiO_2 catalyst is limited to two runs as confirmed by TGA–DSC and elemental analysis. The process of stabilizing Hemin on TiO_2 surface is under progress.

Acknowledgements

Authors acknowledge the financial assistance from University Grants Commission (UGC) and Department of Science and Technology (DST-IDP & DST-SERC), Government of India.

References

[1] A. Molinari, R. Amadelli, L. Antolini, A. Maldoti, P. Battioni, D. Mansuy, Journal of Molecular Catalysis A: Chemical 158 (2000) 521–531.
[2] S.A. Qaradawi, S.R. Salman, Journal of Photochemistry and Photobiology A: Chemistry 148 (2002) 161–168.
[3] X.H. Wang, J.G. Li, H. Kamiyama, Y. Moriyoshi, T. Ishigaki, Journal of Physical Chemistry B 110 (2006) 6804–6809.
[4] R.T. Tom, T.P. Pradeep, Langmuir 21 (2005) 11896–11902.
[5] L.G. Devi, G.M. Krishnaiah, Journal of Photochemistry and Photobiology A: Chemistry 121 (1999) 141–145.
[6] J. Desilvetro, M. Graetzel, L. Kavan, J. Moser, Journal of the American Chemical Society 107 (1985) 2988–2990.
[7] K.S. Finnie, J.R. Bartlett, J.L. Woolfrey, Langmuir 14 (1998) 2744–2749.
[8] K. Nagaveni, M.S. Hegde, G. Madras, Journal of Physical Chemistry B 108 (2004) 20204–20212.
[9] N. Venkatachalam, M. Palanichamy, V. Murugesan, Journal of Molecular Catalysis A: Chemical 273 (2007) 177–185.
[10] R. Rahimi, E.H. Fard, S. Saadati, M. Rabbani, Journal of Sol-Gel Science and Technology 62 (2012) 351–357.
[11] R.A. Larson, J.C. Silva, Environmental Toxicology and Chemistry 19 (2000) 543–548.
[12] A.P. Toor, A. Verma, C.K. Jotshi, P.K. Bajpai, V. Singh, Dyes and Pigments 68 (2006) 53–60.
[13] K. Nagaveni, G. Sivalingam, M.S. Hegde, G. Madras, Applied Catalysis B: Environmental 48 (2004) 83–93.

[14] M. Saquib, M. Muneer, Dyes and Pigments 53 (2002) 237–249.
[15] L.G. Devi, S.G. Kumar, Applied Surface Science 261 (2012) 137–146.
[16] T. Sauer, G. Cesconeto, H.J. Jose, R.F.P.M. Moreira, Journal of Photochemistry and Photobiology A: Chemistry 149 (2002) 147–154.
[17] M. Saquib, M. Muneer, Dyes and Pigments 56 (2003) 37–49.
[18] A. Houas, H. Lachheb, M. Ksibi, E. Elaloui, C. Guillard, J.M. Herrmann, Applied Catalysis B: Environmental 31 (2001) 145–157.
[19] H.J. Benkelberg, P. Warneek, Journal of Physical Chemistry 34 (1995) 5214–5221.
[20] L.G. Devi, K. Nagaraju, S.G. Kumar, Chinese Journal of Chemistry 28 (2010) 2151–2161.
[21] S.O. Obare, T. Ito, G.J. Meyer, Environmental Science and Technology 39 (2005) 6266–6272.
[22] W.Y. Choi, A. Termin, M.R. Hoffmann, Journal of Physical Chemistry 98 (1999) 13669–13679.
[23] S.O. Obare, T. Ito, M.H. Balfour, G.J. Meyer, Nano Letters 3 (2003) 1151–1153.
[24] T. Ohno, Z. Miyamoto, K. Nishijima, H. Kanemitsu, F. Xueyuan, Applied Catalysis A: General 302 (2006) 62–68.
[25] M. Mrowetz, E. Selli, Journal of Photochemistry and Photobiology A: Chemistry 162 (2004) 89–95.
[26] N. Murakami, A. Ono, M. Nakamura, T. Tsubota, T. Ohno, Applied Catalysis B: Environmental 97 (2010) 115–119.
[27] L.G. Devi, S.G. Kumar, K.M. Reddy, C. Munikrishnappa, Journal of Hazardous Materials 164 (2009) 459–467.
[28] L.G. Devi, K.E. Rajashekhar, K.S. Anantha Raju, S.G. Kumar, Journal of Molecular Catalysis A: Chemical 314 (2009) 88–94.